Applied Mathematical Modelling 36 (2012) 2178–2191

Contents lists available at SciVerse ScienceDirect

Applied Mathematical Modelling

journal homepage: www.elsevier.com/locate/apm

Motion measurement of a two-wheeled skateboard and its dynamical simulation

Satoshi Ito *, Shouta Takeuchi, Minoru Sasaki

Department of Human and Information systems, Faculty of Engineering, Gifu University, Yanagido 1-1, Gifu 501-1193, Japan

ARTICLE INFO

Article history:
Received 25 February 2011
Received in revised form 2 August 2011
Accepted 9 August 2011
Available online 8 September 2011

Keywords:
Skateboard
Propulsion
Motion measurement
Dynamical model
Simulation

ABSTRACT

This study investigates the dynamics of the propulsion mechanism of a two-wheeled skateboard by measurements of human skateboard motion and computer simulations using a simplified model. This model expresses the board motion within the horizontal plane. The inputs of the model are the yaw moment about a vertical axis, horizontal force normal to the skateboard axis, and two-wheel orientations, while the outputs are the center of mass position in the horizontal plane and the board orientation. By selecting parameters of sinusoidal inputs to fit the measurement data, similar output data is obtained from the motion measurements and computer simulations. This result allows us to conclude that some sinusoidal motions and forces can robustly propel this type of skateboard.

1. Introduction

Mobility is an ability to move from one place to another and allows biological systems to enlarges their activity area. To achieve mobility, wheeled systems are occasionally utilized, which enable faster spatial movement than legged systems on a flat terrain.

Some wheels in automobiles are active, i.e., are directly driven by an engine or a motor. Although active wheels are convenient for controlling the speed, all the wheels should not be necessarily active; the active wheels require complex mechanisms for drive transmission, which not only increases the weight but also includes some parts causing mechanical troubles by wearing. More energies are required to drive many wheels. Therefore, passive wheels are partially adopted in some wheeled systems.

The rotation of the passive wheels requires some kinds of forces from the outside instead of the direct driving force of the wheel axis. A roller skate is an example of a device that consists of all passive wheels, where the propelling power is produced from the leg motion kicking the ground: the wheels under the supporting leg rotate by the propulsion of ground reaction force which the other leg generates by directly pushing the ground backward. However, the effective use of degrees of freedom (DOF) of motion of a mechanism mounted on passive-wheel systems can propel the wheeled system without kicking the ground. Skateboards [1,2], snakeboards [3] or other vehicles are examples of such systems [4–7]. Especially, the snakeboard was studied much by Ostrowski and Burdick [8–10], Marsden and Ostrowski [11], Ostrowski [12], Ostrowski et al. [13], McIsaac and Ostrowski [14], and was discussed much from viewpoint of dynamics reduction [15–17], structure of dynamics [18–23], controllability [24], stabilization of numerical solutions [25] or non-holonomic control [26–36].

* Corresponding author.
E-mail address: satoshi@gifu-u.ac.jp (S. Ito).

0307-904X/$ - see front matter © 2011 Elsevier Inc. All rights reserved.
doi:10.1016/j.apm.2011.08.005

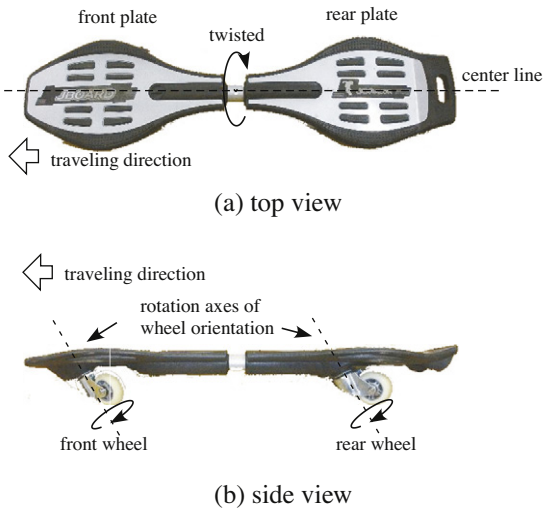

Fig. 1. Two-wheeled skateboard. It consists of two plates, front and rear, which can be twisted around the center line. The wheel is attached on the center line at each plate. The rotation axis of the wheel orientation inclines backward.

Recently, a new type of two-wheeled skateboard has become available in the market, which has an additional degree of freedom around its roll axis, as shown in Fig. 1. Two wheels are attached to the center line of the board: one to the front plate and the other to the rear plate. The rotation axes of each wheel orientation are inclined backward, which defines the traveling direction of the board (to the left in this figure) since wheel orientation is restricted. The rider who is facing sideways of the board places a foot on each plate. In this way, the board moves in the lateral direction of the rider. To propel the board, the rider repeatedly moves his foot back and forth alternatingly relative to the waist with keeping the contact to the board, which provides yaw moment to the board about a vertical axis. In addition, the two plates are twisted around the roll axis by changing the action point of the body weight at each foot. This twist affects the direction of the two wheels because of the backward inclination of the orientation axis.

This type of skateboard can be smoothly accelerated from a stationary state. For acceleration of the board, both the yaw moment from the rider on the board and the twist between the two plates are important. The twist around the roll axis allows one to change the orientation of the two wheels; such an active control of the wheel orientation seems to contribute to rapid traveling motion by facilitating steering actions, because the wheel orientation perpendicular to the propulsion prevents the board from running, while the parallel wheel orientation helps it to go ahead.

Based on the above characteristics, we are investigating the propulsion mechanism of this kind of two-wheeled skateboard. At the first step, the goal of this paper is set to clarify what kind of human inputs is crucial and what kind of input trajectories can successfully propel the board by considering how the yaw moment works and how the twist of the plate should be treated from the aspect of steering the wheel orientation. The replay of a successful skateboard motion is needed at first to investigate its propulsion mechanism, which follows the clarification of the inputs and their trajectories. Therefore, the goal in this paper is one of the important factors for our purpose.

2. Method

In this study, we take the following steps based on both motion measurements and dynamical simulations:

(1) The two-wheeled skateboard is described using a reduced-order model in order to focus only on the propulsion inputs to the board. In this reduced-order model, the "inputs" are yaw moment around the center of mass (CoM) of the board, normal force (the force exerted to the CoM that is normal to the board orientation), and wheel direction.
(2) To investigate what kind of input trajectory can propel the skateboard, skateboard motions are measured. This is a pilot experiment for rough estimation of the input trajectory.
(3) Using data from these measurements, trajectories of the inputs (except the yaw moment) are constructed by function approximation.
(4) Next, these input trajectories are applied to a computer simulation, whose dynamics are derived from a previous reduced-order model with the velocity constraints of the wheel (wheel does not slip to the wheel axis direction).
(5) Then, parameters of the yaw moment are selected, so that the simulation results match the measured data well.

Using these steps, we clarify the inputs from the rider that successfully propel the skateboard in the form of time-varying trajectories.

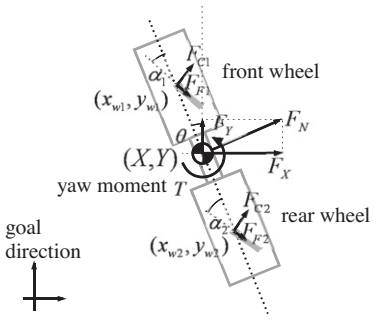

Fig. 2. Two dimensional model of the two wheeled skateboard. The coordinate frame is defined so that the y axis coincides to the central axis of the initial skateboard position, and the x axis becomes normal to the y axis. (X, Y) is the CoM of the skateboard, θ is the orientation of its central axis from the y axis, (X_{wi}, Y_{wi}) is a wheel position, α_i is an orientation of the front and rear wheel, F_X and F_Y are respectively the force form the rider on the board in the x and y direction, F_N is its normal component to the current skateboard orientation, T is a moment from the rider, F_{ci} and F_{Fi} is a component of the ground reaction force at the wheel in the normal and tangential to the wheel direction. Here, $i = 1, 2$ in which $i = 1$ denotes front side, and $i = 2$ does rear side.

3. A reduced-order model

The two-wheeled skateboard has many DOFs: plate twist, wheel orientations, lateral balance, and wheel rotation. To simplify the motion analysis, we assume the following:

- The lateral balance of the board is controlled by the rider's waist extension/flexion, independent of the propulsion, implying that this DOF can be ignored when only the propulsion motion is considered.
- The board can be twisted around its central axis. The weighted position of each of the rider's feet out of the central axis twists two plates each other. This twist affects the orientation of the wheels. Thus, if the wheel orientation is directly regarded as input instead of the weighted position, the twist between the plates is ignored.
- The alternatingly back-and-forth motion of the rider's feet on the board never produces net force parallel to the board orientation because the parallel forces are canceled each other following the action–reaction law of the force. This means that both the yaw moment and normal force are input forces from the rider.

Based on these assumptions, the board motion is expressed by a two-dimensional model, as illustrated in Fig. 2. The motion of this model is described by a first-order, six-dimensional, differential equation with two velocity constraints (see Appendix A).

In this motion equation, the inputs to the board are the yaw moment T, the normal force to the board F_N, and the wheel orientations α_1 and α_2. To simulate the board motions, a time profile of these inputs is required. We obtain them except T by approximating measurement data of the skateboard motion, and determine T so that the measurement data and the simulation data will match well.

4. Motion measurement of a two-wheeled skateboard

4.1. Objective and measurement conditions

The objective of this measurement is to identify the inputs to the board: the yaw moment T, the net horizontal force F_N normal to the board orientation, (which are applied around/to CoM of the board by both feet), and the wheel orientations α_1 and α_2.

The board motion was measured by a motion-capture system as shown in Fig. 3. This system has four high-speed cameras, which capture 640×480 pixel images at 120 frames per second. A flat area of approximately 0.5 m $\times$ 3 m was prepared as measurement space, so that all markers would always be captured by at least two cameras. To detect the board motion, three markers were attached. The first marker was attached to the center of the board, because the center of mass (CoM) of the board is located here due to the symmetrical board structure. To detect the wheel orientation, the marker should have been attached just above the joint of the two-wheel caster. However, the feet of the subject were placed at this position, so the marker was attached to two toes of the subject. A 41-year-old male subject, weighing 65 kg, was asked to propel the board from the rest state and then to maintain straight motion until the end of the measurement area for a constant period. The feet of the subject were placed at the center of the two plates, so that the markers were as close to the joint center of the wheel orientation as possible, and the line connecting the two markers was parallel to the board.

Five trials were conducted under the above conditions. These measurements were executed with permission (No. 21–127) from the ethics committee of our organization.

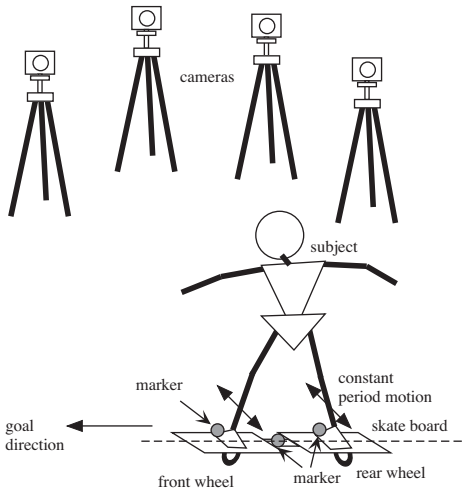

Fig. 3. Measurement setup. Motion capture system with four cameras measures the position of the three markers attached on the center of the skateboard and toes of the subject in every 1/120 s.

4.2. Data processing and results

Let P_C, P_L and P_R be marker positions attached to the center of the board, the left toe, and the right toe, respectively, as shown in Fig. 4. The board direction θ is obtained from the angle between the line $\overline{P_L P_R}$ and the goal direction.

In contrast, the board CoM position, velocity, and acceleration are automatically obtained from the motion-capture system based on P_C's captured data by numerical difference operation without filter (a band-pass filter is applied later). Multiplying the mass by its acceleration data, the force from the subject to the board F_X is obtained (see Appendix B). Using the board orientation θ, the normal force F_N can be computed as

$$F_N = F_X / \cos\theta. \tag{1}$$

The wheel orientations α_1 and α_2 are approximated as those of the velocity vectors of the markers on the toes by assuming that the distance between the rotation joint and the marker is sufficiently small. Thus, the wheel orientations are computed by

$$\alpha_1 = \tan^{-1}\left(\frac{V_{Lx}}{V_{Ly}}\right) - \theta, \tag{2}$$

$$\alpha_2 = \tan^{-1}\left(\frac{V_{Rx}}{V_{Ry}}\right) - \theta. \tag{3}$$

Here, $V_L = (V_{Lx}, V_{Ly})$ and $V_R = (V_{Lx}, V_{Ly})$ are the velocity vector of P_L and P_R, respectively.

The yaw moment T cannot be measured using this measurement setup. Thus, T was identified so that the simulation result computed using its dynamical model in Section 3 matches the measured trajectory of the board traveling in the goal direction.

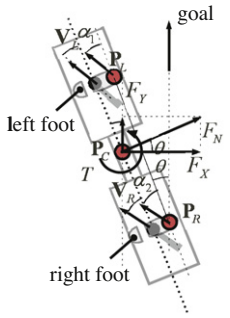

Fig. 4. Input calculation. In this figure, P_C, P_L and P_R are marker positions attached respectively to the center of the board, the left toe, and the right toe, and V_L and V_R are the velocity vector of the marker P_L and P_R, respectively.

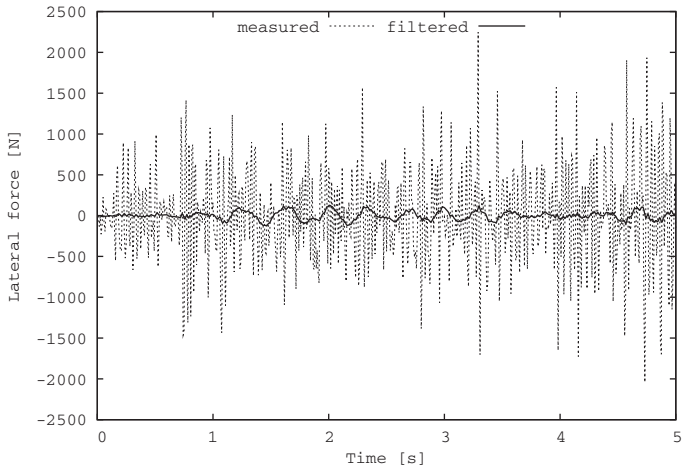

(a) Lateral force

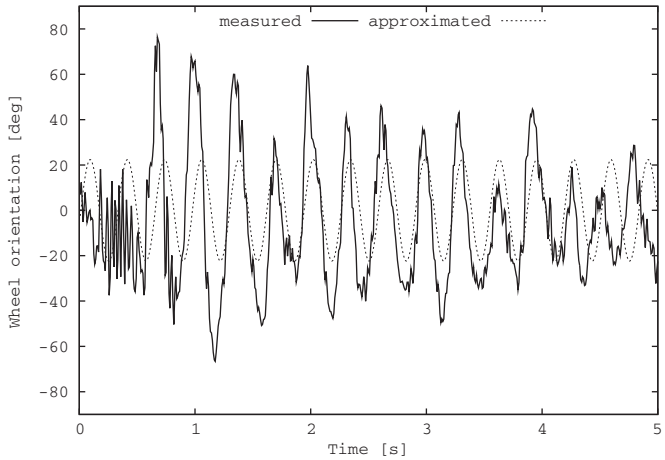

(b) Front wheel orientation α_1.

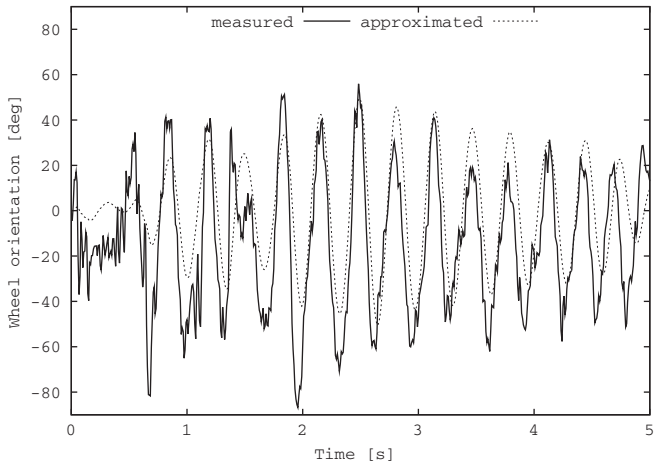

(c) Rear wheel orientation α_2.

Fig. 5. Measurement result of the board motion.

4.3. Results

The values of F, α_1 and α_2, which are computed from the three markers' information, are depicted by solid lines in each graph of Fig. 5. This is the last of the five trials, and the best data in the sense that the period variation of the data in α_1 and α_2 is small, as seen in the next section.

5. Input trajectory construction

5.1. Sinusoidal input approximation

In this section, we construct approximated curves of each input: the normal force and the wheel directions. The obtained curves will be utilized as the input of the computer simulation.

Because of the periodicity, sinusoidal functions are used to make approximated curves of the measurement data obtained in the previous section, because the sinusoidal functions are compatible with the frequency analysis we adopt later.

It is natural to assume that the frequencies are the same for all the inputs as an output, i.e., a periodic skateboard motion. Thus, we utilize the following functions for each input:

$$\alpha_1 = \hat{\alpha}_{1A}\sin(2\pi\hat{f}t + \hat{\phi}_1), \tag{4}$$

$$\alpha_2 = -\hat{\alpha}_{2A}\sin(2\pi\hat{f}t + \hat{\phi}_2), \tag{5}$$

$$F_N = \widehat{F}_A\sin(2\pi\hat{f}t + \hat{\phi}_F), \tag{6}$$

$$T = \widehat{T}_A\sin(2\pi\hat{f}t + \hat{\phi}_F). \tag{7}$$

Here, it is assumed that F and T have the same phase shift $\hat{\phi}_F$ because they are originally generated from the same motions, that is, the alternating back-and-forth motions of both feet on the board with a contact that are usually a half-period out of phase.

In the above equations, unknown parameters are frequency $\hat{f}$, the amplitudes $\widehat{F}_A$, $\widehat{T}_A$, $\hat{\alpha}_{1A}$, $\hat{\alpha}_{2A}$ and the phase lags $\hat{\phi}_F$, $\hat{\phi}_1$, $\hat{\phi}_2$.

5.2. Frequency estimation

In order to identify the frequency of the motion, spectrum analysis was performed. The frequency should be detected from the input signals because the periodic board motion is produced from such input signals. However, there is no data for the yaw moment, and the normal force is noisy because it is computed by differentiating the CoM position data. This is the reason why the data of two wheel directions was utilized.

The peak frequencies, i.e., the dominant frequency in terms of the frequency domain power plot, should be match in the front and rear wheel orientations; however, it usually fluctuated in actual measurement data. Thus, the average of two peak frequencies was selected as the peak frequency of the board motion.

5.3. Phase-shift estimation

Next, the phase shifts were identified based on cross-correlation. Each input data was initially filtered through a two-order band-pass filter, whose peak frequency was set as that detected in the previous section. This filtering prevents unrelated frequency components from correlating. Next, the filtered data were cross-correlated to the sine wave with a phase shift of zero at 0 s. The maximal point of the cross-correlation value was selected as the phase shift of the data.

5.4. Amplitude estimation

Finally, the amplitude was identified using least mean square method. This method was selected in order to minimize the squared sum of the error between the sinusoidal approximation and the measured signals. The signals to be matched were filtered once in Section 5.3, extracted from 2 s until the end. Before this period, the motions were transient, while those during this period were regarded almost steady in all the measurements.

Because an unknown parameter, amplitude, is given as a linear coefficient in the input–output relation, the pseudo-inverse was applied to the estimation.

5.5. Results

The power spectrum of this data is shown in Fig. 6. The estimated motion frequencies are listed in Table 1 along with the other parameters. The sinusoidal graphs using these parameters are depicted by dotted lines in both Figs. 5 and 7.

Currently, three input signals, two wheel orientations (4) and (5), and the normal force (6) have been obtained. The yaw moment will be estimated in the next section, based on computer simulations.

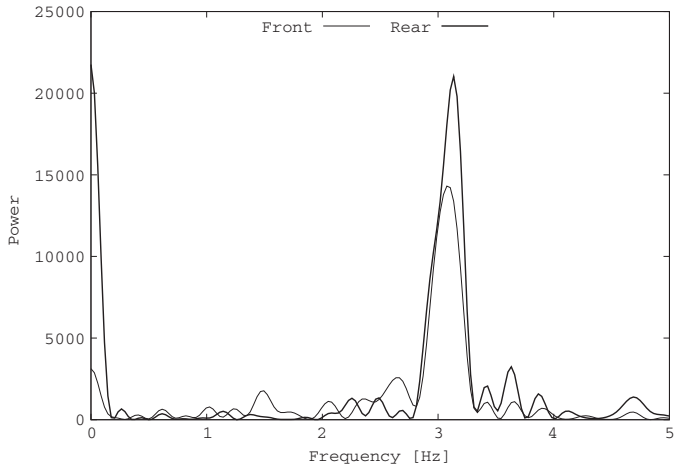

Fig. 6. Power spectrum of two wheel deviation.

Table 1
Estimated parameters. $\hat{f}$ is an estimate of the skateboard motion, $\hat{\phi}_1$, $\hat{\phi}_2$ and $\hat{\phi}_F$ is estimates of the phase lag of the front wheel motion, the rear wheel motion, and the normal force, respectively, $\hat{\alpha}_{A1}$ and $\hat{\alpha}_{A2}$ are estimates of the amplitude of the front and rear wheel rotation, respectively, $\widehat{F}_A$ and $\widehat{T}_A$ are estimates of the amplitude of the normal force and yaw moment, respectively.

	$\hat{f}$ [Hz]	$\hat{\phi}_1$ [°]	$\hat{\phi}_2$ [°]	$\hat{\phi}_F$ [°]	$\hat{\alpha}_{A1}$ [°]	$\hat{\alpha}_{A2}$ [°]	$\widehat{F}_A$ [N]	$\widehat{T}_A$ [Nm]
1st	2.89	138.4	147.7	10.4	15.0	32.1	−105.5	10.2
2nd	2.94	114.3	140.8	132.3	23.3	32.9	−34.1	4.6
3rd	2.87	0.00	43.3	8.7	21.5	19.6	−33.4	3.1
4th	2.48	51.8	29.5	37.5	11.6	12.4	13.8	6.9
5th	3.11	−15.2	19.0	−5.1	22.4	27.8	−33.8	3.7

6. Simulation for torque estimation

The yaw moment cannot be measured in our experimental setup. Here, we estimate it using dynamical simulations of a reduced-order model, as described in Section 3.

Only one unknown parameter exists: the amplitude of the yaw moment $\widehat{T}_A$. Several parameter values were tried and then examined to determine whether the traveling distance in the goal direction matches the measurement data well, in the sense that the least mean square of the error between the measurement and simulation data is small. In fact, $\widehat{T}_A$ was changed in increments of 0.1 N m.

For the simulation, a fourth-order Runge–Kutta method was applied with the step size 1/120 s. The parameters that were set based on the actual board as well as the subject are shown in Appendix C.

The optimal values in each trial are also shown in the rightmost row of Table 1. In addition, the simulation results using input signals (6) and (5) with the parameters of the fifth trial in Table 1 are depicted in Fig. 8. Although the simulated and measured data of the lateral deviation and the board orientation did not matched well, the traveling distance to the goal direction, which was selected for the evaluation for parameter estimation, showed similar trajectories.

These results demonstrate that the sinusoidal inputs for two-wheel orientations, normal force, and the yaw moment could propel a reduced-order model of a two-wheeled skateboard.

7. Discussion

The sinusoidal inputs constructed from the measurement data successfully drove the reduced-order model of the two-wheeled skateboard. The trajectory of the board's traveling direction matched the measurement data well. This fact implies that if a human produces the forces by foot back-and-forth motions and steers the front and rear wheels in a sinusoidal manner, he can probably propel this board.

To investigate the robustness of this motion, parameters related to the input signals were changed one at a time in some ranges. The centered values are $\hat{f} = 3$ [Hz], $\widehat{F}_A = -30$ [N], $\widehat{T}_A = 4$ [Nm], $\hat{\alpha}_{1A} = 20$ [°], $\hat{\alpha}_{2A} = 25$ [°], $\hat{\phi}_F = 0$ [°], $\hat{\phi}_1 = 0$ [°], and $\hat{\phi}_2 = 0$ [°]. A traveling distance, i.e., the forward position over the first 5 s when starting from zero velocity, is shown in Fig. 9. As expected, large wheel amplitude and yaw moment allow the board to travel a long distance, while the effect of the lateral force on the traveling direction is small. The traveling distance changes symmetrically with the phase difference: the changes to the traveling distance are almost the same leads and lags of the same phase. In addition, the traveling distance

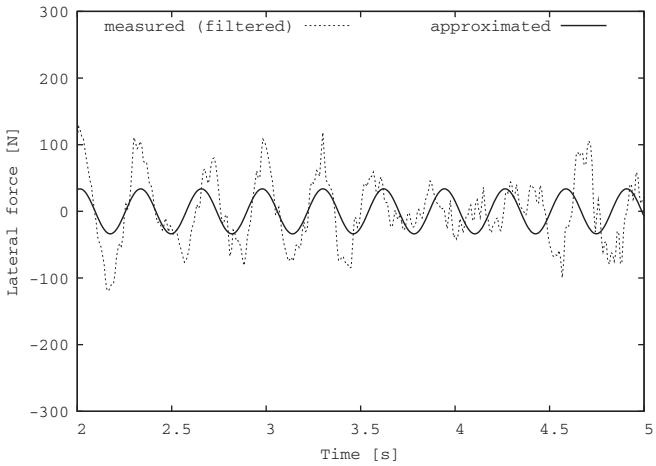

(a) Normal force

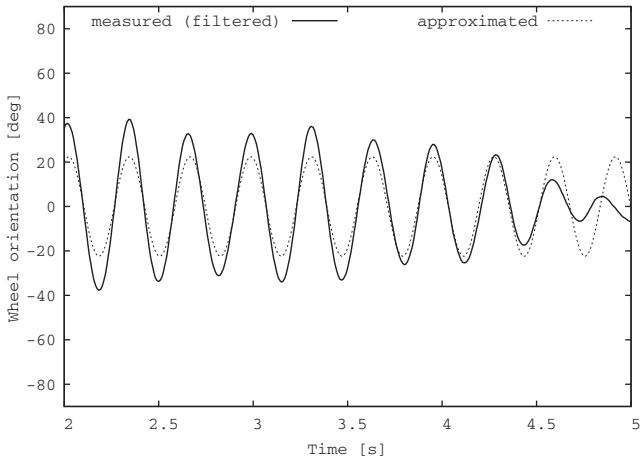

(b) Front wheel orientation α_1.

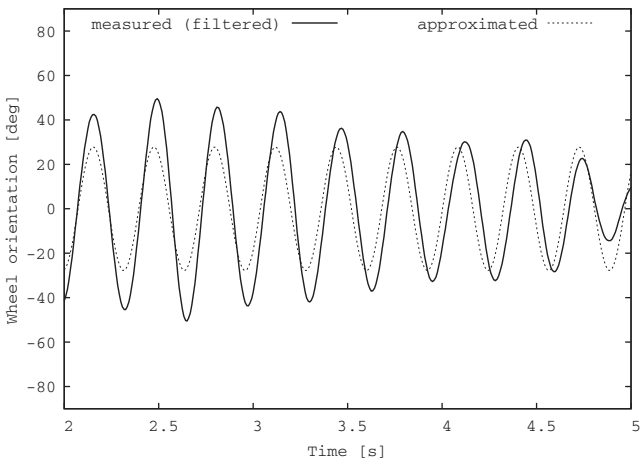

(c) Rear wheel orientation α_2.

Fig. 7. Input reconstruction with filtered data.

increases because of the phase difference of the rear wheel, while it decreases because of that of the front wheel. This indicates that the wheel should be oriented so that the yaw moment is easily produced, that is, for a positive counter-clockwise

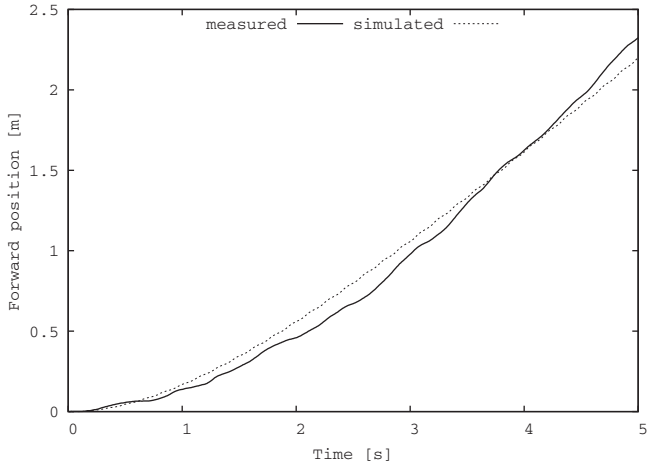

(a) Goal direction.

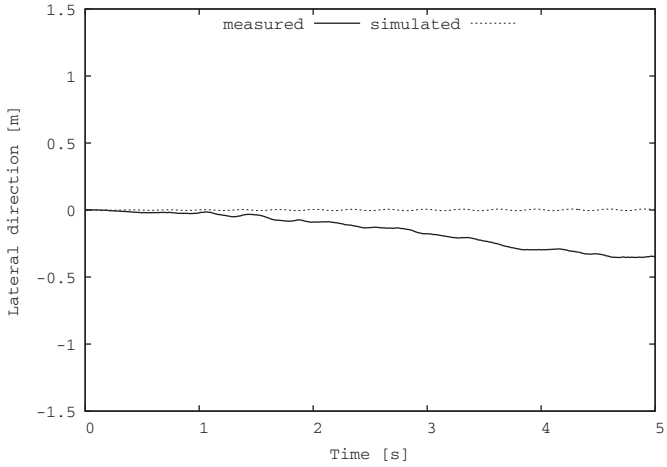

(b) Normal deviation.

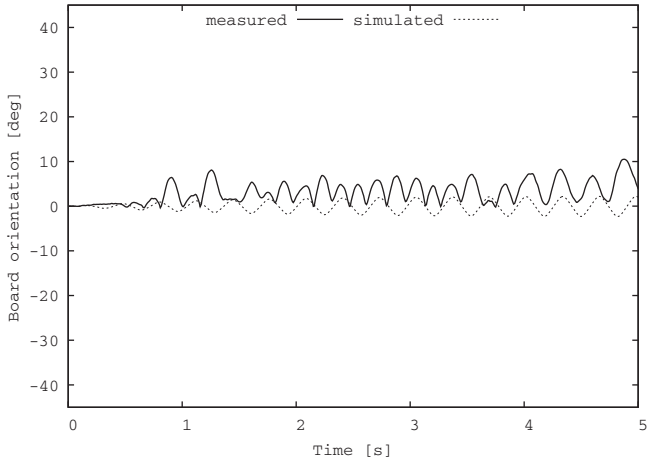

(c) Board orientation.

Fig. 8. Comparison of simulation results from reconstruct inputs with measurement data.

moment, the front wheel should face left, while the rear one should face right at the start. Some combination of the phasic relations as well as the amplitude among inputs produces the backward motions, which may provide us with some hints of

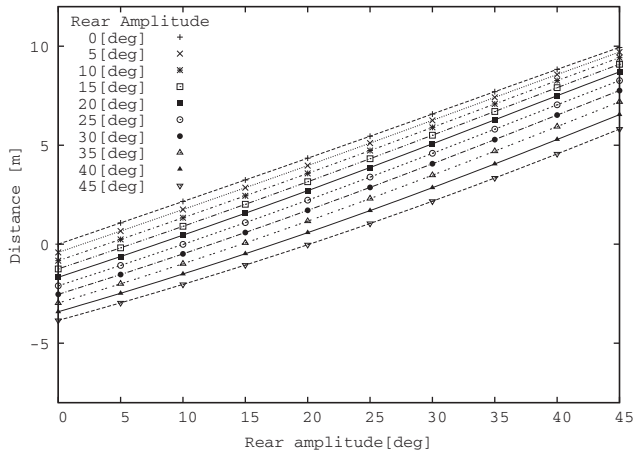

(a) wheel amplitude.

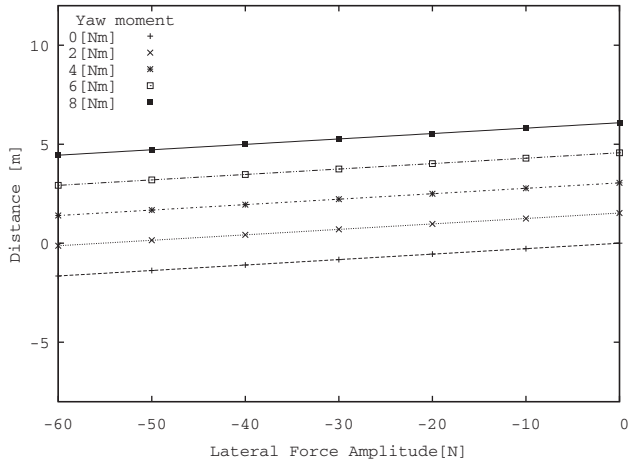

(b) lateral force and yaw moment.

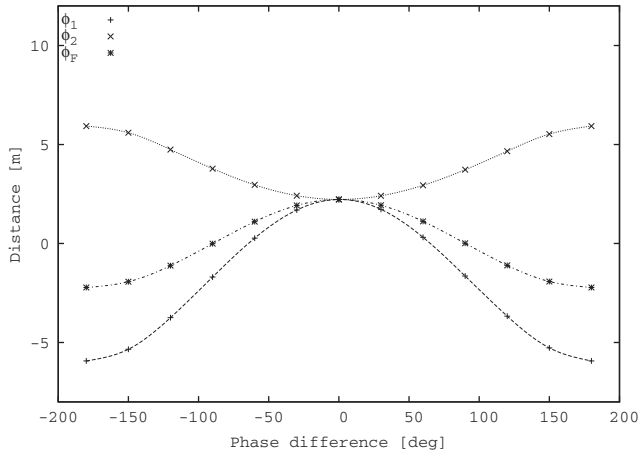

(c) phase difference.

Fig. 9. Traveling distance with respect to parameter variations. ϕ_1, ϕ_2 and ϕ_F are the initial phase lags of the input for the front wheel orientation, rear wheel orientation and the normal force (yaw moment).

propulsion mechanism of skateboard. Anyway, independent of the deviation of several parameters, the sinusoidal inputs can propel the board, indicating the robustness of the sinusoidal propulsion with respect to the parameter variations.

The coincidence of the time-based trajectory to the goal direction implies the validity of the dynamical model of the two-wheeled skateboard. However, the variation of the estimated parameters is not so small. In Table 1, although the motion frequency is commonly 3 Hz, positive and negative values are found for the other parameters. In the first trial, where the data largely deviates from the other trials, a multipeak curve was observed (which is not shown in this paper). This fluctuation of the motion frequency enlarges the phase deviation in the sinusoidal approximation from the measured data. Consequently, a slight decline in the frequency largely affects the phase and amplitude estimation. To obtain consistent data, it is desirable that the subject is proficient in producing the precise periodic motion of the skateboard.

In addition, the final confirmation of the model validity requires the measurement of the yaw moment in order to compare the estimated value from the simulations. Our experimental setup does not provide this data. In the future, we will introduce a measurement system for the yaw moment in order to complete the modeling process.

8. Conclusion

Mobility based on the passive wheel has some advantages in terms of cost and safety. Skateboards are a type of mobility with passive wheels. Of the various types of skateboards, a two-wheeled skateboard was considered in this study because this type of skateboard can be driven without kicking the ground, that is, by using only body motions on the board.

In order to investigate the dynamics of the propulsion mechanism, both computer simulations and motion measurements were adopted. For the computer simulations, a reduced-order model was introduced, assuming that lateral balance is always maintained by human-waist extension/flexion, and that the wheel orientations are determined by the CoP of each foot direction twisting the board body. The inputs of this dynamical model are defined as a yaw moment, a normal force, and two-wheel orientations, while the outputs are the CoM position in the horizontal plane and the board orientation. This modeling is deferent from the snakeboard in a point that the normal force to the board is taken into account.

To propel this model, the input data is obtained from the measurement of the human skateboard motion. Because of the periodicity of the motions, the input data was approximated by sinusoidal functions. Simulation results from these input trajectories produced similar output data (that is, skateboard trajectories) to the measured data. Thus, a two-wheeled skateboard can be propelled by applying force and moment in a sinusoidal manner. Although some studies on snakeboard tried sinusoidal inputs in simulations by change the frequency ratio [8,34,33], this paper originally examined the phase relation between wheel orientation and yaw moment as well as the effect of a newly-introduced normal force to the forward motion, and demonstrated that phasic relations affect the traveling distance, symmetrically.

Now, we have obtained a reduced-order model that can describe board propulsion well. In future, we will analytically clarify the propulsion mechanism using this reduced-order model, and then confirm it using a mechanical system, such as robots.

Acknowledgments

Part of this study was supported by 'Gifu University Activation Grant' and Japan Society for the Promotion of Science, 'Grant-in-Aid for Scientific Research (C) No. 22500173'.

Appendix A. Motion equation

A.1. Body dynamics

In a reduced-order model of a two-wheel skateboard, it is assumed that the board is symmetrical in the lateral direction, and thus, the CoM is assumed to be located at the central axis of the board. Furthermore, the center of the wheel orientation is also located at the central axis, although it is actually deviated because of the eccentricity of the wheel as well as the backward inclination of the axis for the orientation. Under these assumptions, a motion equation of this model is represented in the horizontal space as

$$M\ddot{Q} = A_C^T F_C + A_F^T F_F + T, \tag{A.1}$$

$$Q = [X \quad Y \quad \theta]^T, \tag{A.2}$$

$$M = \begin{bmatrix} M_b & 0 & 0 \\ 0 & M_b & 0 \\ 0 & 0 & I_b \end{bmatrix}, \tag{A.3}$$

$$T = [F_X \quad F_Y \quad T]^T, \tag{A.4}$$

$$F_C = \begin{bmatrix} F_{C1} \\ F_{C2} \end{bmatrix}, \tag{A.5}$$

$$F_F = \begin{bmatrix} F_{F1} \\ F_{F2} \end{bmatrix}. \tag{A.6}$$

Here, (X,Y) is the CoM position in the horizontal space, θ is the board orientation, M_b is the mass of the board, I_b is its inertia, and F_X, F_Y and T are forces or moments from the human on the board. F_{C1} and F_{C2} are forces that constrain the wheel velocity, F_{F1} and F_{F2} are the viscous friction of the wheel rotation, and A_C and A_F comprise a matrix that is given as

$$A_C = \begin{bmatrix} \cos(\theta+\alpha_1) & \sin(\theta+\alpha_1) & -L_1\cos\alpha_1 \\ \cos(\theta+\alpha_2) & \sin(\theta+\alpha_2) & L_2\cos\alpha_2 \end{bmatrix}, \tag{A.7}$$

$$A_F = \begin{bmatrix} \sin(\theta+\alpha_1) & -\cos(\theta+\alpha_1) & -L_1\sin\alpha_1 \\ \sin(\theta+\alpha_2) & -\cos(\theta+\alpha_2) & L_2\sin\alpha_2 \end{bmatrix}, \tag{A.8}$$

where L_1 and L_2 represent the distance between the CoM to the rotation center of the front and rear wheel orientations, respectively. α_1 and α_2 represent the wheel orientations from the center axis of the board.

A.2. Velocity constraints

The wheels move only in the tangential direction of the wheel orientation, and never in the normal direction. These conditions are described as the following equations:

$$v_{w1} = -\dot{x}_{w1}\sin(\theta+\alpha_1) + \dot{y}_{w1}\cos(\theta+\alpha_1), \tag{A.9}$$
$$v_{w2} = -\dot{x}_{w2}\sin(\theta+\alpha_2) + \dot{y}_{w2}\cos(\theta+\alpha_2), \tag{A.10}$$
$$\dot{x}_{w1}\cos(\theta+\alpha_1) + \dot{y}_{w1}\sin(\theta+\alpha_1) = 0, \tag{A.11}$$
$$\dot{x}_{w2}\cos(\theta+\alpha_2) + \dot{y}_{w2}\sin(\theta+\alpha_2) = 0. \tag{A.12}$$

Here, v_{w1} and v_{w2} represent the speed of the front and rear wheel. (x_{w1},y_{w1}) and (x_{w2},y_{w2}) are the positions of the front and rear wheels in the measurement space (the task-coordinate frame), and are given as

$$x_{w1} = X - L_1\sin\theta, \tag{A.13}$$
$$y_{w1} = Y + L_1\cos\theta, \tag{A.14}$$
$$x_{w2} = X + L_2\sin\theta, \tag{A.15}$$
$$y_{w2} = Y - L_2\cos\theta, \tag{A.16}$$

Substituting (A.9)–(A.12) by (A.13)–(A.16), the following equations are obtained:

$$V_w = \begin{bmatrix} v_{w1} \\ v_{w2} \end{bmatrix} = -A_F\dot{Q}, \tag{A.17}$$

$$A_C\dot{Q} = 0. \tag{A.18}$$

Eq. (A.19) in the next section describes the velocity constraints of the wheel movement.

A.3. Motion equation with velocity constraints

The following equation is obtained by differentiating (A.18) with respect to time:

$$A_C\ddot{Q} + \dot{A}_C\dot{Q} = 0, \tag{A.19}$$

where

$$\dot{A}_C = \begin{bmatrix} -\dot{\theta}\sin(\theta+\alpha_1) & \dot{\theta}\cos(\theta+\alpha_1) & 0 \\ -\dot{\theta}\sin(\theta+\alpha_2) & \dot{\theta}\cos(\theta+\alpha_2) & 0 \end{bmatrix}. \tag{A.20}$$

In addition, the viscous friction is described as

$$F_F = BV_w = -BA_F\dot{Q}, \tag{A.21}$$

$$B = \begin{bmatrix} b_1 & 0 \\ 0 & b_2 \end{bmatrix}, \tag{A.22}$$

where b_1 and b_2 represent the viscous coefficient of the rotation of the front and rear wheel, respectively.

From (A.1), (A.19) and (A.21), the motion equation with velocity constraints is given as follows:

$$\begin{bmatrix} M & -A_C^T \\ -A_C & O \end{bmatrix} \begin{bmatrix} \ddot{Q} \\ F_C \end{bmatrix} = \begin{bmatrix} -A_F^T B A_F \\ \dot{A}_C \end{bmatrix} \dot{Q} + \begin{bmatrix} T \\ O \end{bmatrix}. \tag{A.23}$$

Appendix B. Lateral force calculation

The motion equation of the board is given in (A.1). To determine F_X, F_Y and T from the measured data, the motion of the human is also considered in the horizontal space. Based on the law of action and reaction, its motion equations are

$$M_h \ddot{X}_h = -F_X, \tag{B.1}$$

$$M_h \ddot{Y}_h = -F_Y, \tag{B.2}$$

$$I_h \ddot{\theta}_h = -T, \tag{B.3}$$

where (X_h, Y_h) is the human's CoM position in the horizontal space, θ_h is the orientation, M_h is the mass, and I_h is the inertia. Here, suppose that the CoM of the board and the human always coincide in the X direction during the motion, that is, $X \sim X_h$. Then,

$$F_X \approx -M_h \ddot{X}. \tag{B.4}$$

Thus, the force from the human in the X direction is detected from the acceleration data of the board CoM in the X direction. In this study, the normal force was actually obtained based on the relation (6).

The torque from the human, on the other hand, cannot be detected, because the human on the board twists his waist to drive the board, implying that $\theta_b \neq \theta_h$. Therefore, the approximated method for F_X detection is not applied to the torque detection.

Appendix C. Parameters in simulation

In the computer simulation discussed in this study, the following parameter values were set: $M_b = 5$ kg, $M_h = 65$ kg, $L_1 = L_2 = 0.3$ m, $b_1 = b_2 = 1.5$ Ns/m, $I_b = M_b(l^2 + w^2)/12$. Here, $l = 0.8$ m is the board length and $w = 0.2$ m is the board width. Initial values of the simulations are: $x(0) = y(0) = \theta(0) = \dot{x}(0) = \dot{y}(0) = \dot{\theta}(0) = 0$.

References

[1] M. Hubbard, Human control of the skateboard, Journal of Biomechanics 13 (1980) 745–754.
[2] Y. Ispolov, B. Smolnikov, Skateboard dynamics, Computer Methods in Applied Mechanics and Engineering 131 (3–4) (1996) 327–333.
[3] A. Lewis, J. Ostrowski, J. Burdick, R. Murray, Nonholonomic mechanics and locomotion: the snakeboard example, in: Proceedings of the 1994 IEEE International Conference on Robotics and Automation, 1994, pp. 2391–2400.
[4] A. Lewis, Simple mechanical control systems with constraints, IEEE Transactions on Automatic Control 45 (8) (2000) 1420–1436.
[5] K.M. Lynch, Optimal control of the thrusted skate, Automatica 39 (1) (2003) 173–176.
[6] S. Chitta, P. Cheng, E. Frazzoli, V. Kumar, Robotrikke: a novel undulatory locomotion system, in: IEEE International Conference on Robotics and Automation, vol. 2, Citeseer, 2005, p. 1597.
[7] A. Astolfi, R. Ortega, A. Venkatraman, A globally exponentially convergent immersion and invariance speed observer for mechanical systems with nonholonomic constraints, Automatica 46 (1) (2010) 182–189.
[8] J. Ostrowski, J. Burdick, Geometric perspectives on the mechanics and control of robotic locomotion, in: Proceedings of International Symposium on Robotics Research, vol. 7, Citeseer, 1996, pp. 536–547.
[9] J. Ostrowski, J. Burdick, Controllability tests for mechanical systems with symmetries and constraints, Journal of Applied Mathematics and Computer Science 7 (2) (1997) 101–127.
[10] J. Ostrowski, J. Burdick, The geometric mechanics of undulatory robotic locomotion, The International Journal of Robotics Research 17 (7) (1998) 683–701.
[11] J. Marsden, J. Ostrowski, Symmetries in motion: geometric foundations of motion control, Nonlinear Science Today (1998) 1–21.
[12] J. Ostrowski, Steering for a class of dynamic nonholonomic systems, IEEE Transactions on Automatic Control 45 (8) (2000) 1492–1498.
[13] J. Ostrowski, J.P. Desai, V. Kumar, Optimal gait selection for nonholonomic locomotion systems, The International Journal of Robotics Research 19 (3) (2000) 225–237.
[14] K. McIsaac, J. Ostrowski, Motion planning for anguilliform locomotion, IEEE Transactions on Robotics and Automation 19 (4) (2003) 637–652.
[15] W. Koon, J. Marsden, The Hamiltonian and Lagrangian approaches to the dynamics of nonholonomic systems, Reports on Mathematical Physics 40 (1) (1997) 21–62.
[16] W. Koon, J. Marsden, Poisson reduction for nonholonomic mechanical systems with symmetry, Reports on Mathematical Physics 42 (1) (1998) 101–134.
[17] O. Fernandez, T. Mestdag, A. Bloch, A Generalization of Chaplygin's Reducibility Theorem, 2009. Available from: <arXiv:0909.4018>.
[18] A. Bloch, P. Krishnaprasad, J. Marsden, R. Murray, Nonholonomic mechanical systems with symmetry, Archive for Rational Mechanics and Analysis 136 (1) (1996) 21–99.
[19] H. Cendra, J. Marsden, T. Ratiu, Geometric mechanics, Lagrangian reduction and nonholonomic systems, Mathematics Unlimited-2001 and Beyond (2001) 221–273.
[20] M. Kobayashi, W. Oliva, A note on the conservation of energy and volume in the setting of nonholonomic mechanical systems, Qualitative Theory of Dynamical Systems 4 (2) (2004) 383–411.
[21] I. Kosenko, M. Loginova, Y. Obraztsov, M. Stavrovskaya, Multibody systems dynamics: Modelica implementation and Bond Graph representation, in: 5th International Modelica Conference, Vienna, Austria, 2006, pp. 4–5.
[22] S. Ferraro, D. Iglesias, D. de Diego, Momentum and energy preserving integrators for nonholonomic dynamics, Nonlinearity 21 (8) (2008) 1911–1928.
[23] J. Grabowski, M. de León, J. Marrero, D. de Diego, Nonholonomic constraints: a new viewpoint, Journal of Mathematical Physics 50 (2009) 013520.

[24] F. Bullo, M. Zefran, On mechanical control systems with nonholonomic constraints and symmetries, Systems and Control Letters 45 (2) (2002) 133–144.
[25] Z. Terze, J. Naudet, D. Lefeber, Constraint Gradient Projective Method for Stabilized Dynamic Simulation of Constrained Multibody Systems, in: 19th Biennial Conference on Mechanical Vibration and Noise, 2003, pp. 105–113.
[26] S. Martínez, J. Cortes, M. de Leon, Symmetries in vakonomic dynamics: applications to optimal control, Journal of Geometry and Physics 38 (3–4) (2001) 343–365.
[27] S. Iannitti, K. Lynch, Minimum control-switch motions for the snakeboard: a case study in kinematically controllable underactuated systems, IEEE Transactions on Robotics 20 (6) (2004) 994–1006.
[28] S. Martínez, J. Cortés, Motion control algorithms for simple mechanical systems with symmetry, Acta Applicandae Mathematicae: An International Survey Journal on Applying Mathematics and Mathematical Applications 76 (3) (2003) 221–264.
[29] F. Bullo, A. Lewis, Kinematic controllability and motion planning for the snakeboard, IEEE Transactions on Robotics and Automation 19 (3) (2003) 494–498.
[30] P. Vela, J. Burdick, Control of biomimetic locomotion via averaging theory, in: IEEE International Conference on Robotics and Automation, vol. 1, Citeseer, 2003, pp. 1482–1489.
[31] Y. Golubev, A method for controlling the motion of a robot snakeboarder, Journal of Applied Mathematics and Mechanics 70 (3) (2006) 319–333.
[32] E. Shammas, H. Choset, A. Rizzi, Towards automated gait generation for dynamic systems with non-holonomic constraints, in: Proceedings 2006 IEEE International Conference on Robotics and Automation, 2006, pp. 1630–1636.
[33] A. Asnafi, M. Mahzoon, Some flower-like gaits in the snakeboard's locomotion, Nonlinear Dynamics 48 (1) (2007) 77–89.
[34] A. Kuleshov, Further development of the mathematical model of a snakeboard, Regular and Chaotic Dynamics 12 (3) (2007) 321–334.
[35] Manuel de Leon, Juan Carlos Marrero, D. Martin de Diego, 2008. Linear almost Poisson structures and Hamilton–Jacobi equation. Applications to Nonholonomic Mechanics. Available from: <arXiv 801>.
[36] T. Narikiyo, Control of underactuated mechanical systems via passive velocity field control: application to snakeboard and 3D rigid body, Nonlinear Analysis 71 (2009) e2358–e2365.